Adsorption and Decomposition of Formic Acid on Cobalt(0001)

Jeffrey Sims, Cherif Aghiles Ould Hamou, Romain Reocreux, Carine Michel, Javier Giorgi

Adsorption and Decomposition of Formic acid on Cobalt (0001)

Jeffrey J. Sims[a,b], Cherif Aghiles Ould Hamou[a,c], Romain Réocreux[e,f], Carine Michel* [e], Javier B. Giorgi* [a,d]

[a]*Centre for Catalysis Research and Innovation,* [b]*Department of Chemical and Biological Engineering,* [c]*Department of Physics,* [d]*Department of Chemistry and Biomolecular Sciences, University of Ottawa, 10 Marie Curie Pvt., Ottawa, Ontario, Canada. K1N 6N5.*

[e]*Univ Lyon, Ens de Lyon, CNRS UMR 5182, Université Claude Bernard Lyon 1, Laboratoire de Chimie, F-69342, Lyon, France*

[f] Current address: *Thomas Young Centre and Department of Chemical Engineering, University College London, Roberts Building, Torrington Place, London WC1E 7JE, United Kingdom*

*Corresponding authors:
Javier B. Giorgi, jgiorgi@uottawa.ca, 613-562-5800 x 6037
Carine Michel, carine.michel@ens-lyon.fr

Abstract

Formic acid can undergo dehydration or dehydrogenation with variable selectivity over a range of metal catalysts. The selectivity among these reactions depends on the reaction mechanism and reaction conditions pertinent on each surface. This work provides mechanistic insight on the decomposition of formic acid on cobalt at high and low temperature regimes. The adsorption and decomposition of formic acid on a Co(0001) single crystal was studied in ultra-high vacuum by X-ray photoelectron spectroscopy (XPS) and temperature programmed desorption (TPD). Insight is provided using DFT calculations. In the low temperature regime, formic acid adsorbs molecularly on the surface at 130 K. Partial decomposition produces CO at 140 K, and at 160 K the decomposition of formic acid into formate, which is a thermodynamic sink, is dominant. Water can be formed at low temperature via bimolecular processes. At high temperature (>400 K) the similar barriers for decomposition of the formate species lead to the concomitant production of CO, CO_2 and H_2. The correlation between experiment and theory provides a framework for the interpretation of surface species and reaction path operating in different regimes.

1. Introduction

The interaction and reactions of formic acid on transition metal catalysts has been the subject of multiple studies due to the importance of formic acid in a variety of industries.[1–8] Formic acid decomposition possesses similar intermediates as the water-gas shift reaction[9] and methanol oxidation.[10] Additionally, these intermediates are often present in the oxidation of large organic molecules and steam-reforming reactions.[11] As such, formic acid is often a model molecule in the study of bio-oil and biomass applications.[12–14] In addition, formic acid also has been proposed as a hydrogen vector for mobile applications.[15] Hence the importance of understanding and controlling formic acid reactivity has produced a number of fundamental and industrial studies.

Formic acid provides two competing decomposition pathways, namely dehydrogenation and dehydration (eq. 1 and 2). Single crystal investigations of formic acid on transition metal surfaces have shown that not only the ratio of products, but also the mechanism by which they are achieved depends on the nature of the metal and the surface plane involved.[11,16] For example, on Pt(111) formic acid decomposes primarily through the dehydrogenation reaction in UHV[17–19] and the dehydration reaction can only be observed at higher pressures,[20] while on Pt(100) formic acid does not react in UHV conditions.[21] In addition, formic acid has also been suggested to undergo a bimolecular decomposition pathway on Cu,[11,22,23] Ru,[11] and Ni[7,11,23,24] surfaces in addition to or instead of the dehydrogenation and dehydration reactions.

$$HCOOH \rightarrow CO_2 + H_2 \quad (1)$$

$$HCOOH \rightarrow CO + H_2O \quad (2)$$

The decomposition of formic acid on cobalt surfaces are of particular importance because cobalt is a prevalent catalyst for the water-gas shift reaction,[9] and methanol oxidation reaction,[10] as well as being used as an additive to increase performance and stability of direct formic acid/methanol fuel cell catalysts.[8,25–32] Cobalt has also been suggested as desirable catalyst for steam reforming. Despite its importance, a small number of experimental studies of formic acid decomposition on cobalt have been performed. Inglis and Taylor[23] studied the decomposition of formic acid on 1st row transition metal thin films under 30 Torr of formic acid and temperatures between 100-300 ºC. They report a CO_2:CO ratio of approximately 1:1 on cobalt catalysts. Inglis and Taylor also found that this ratio was independent of temperature for the temperature range used in their experiments. They postulated that formic acid may decompose through a bimolecular pathway, but no mechanistic information or reaction pathways were proposed. Tang et al.[33] provided insight by measuring reaction products obtained from metallic cobalt powders and performing TPD and IR spectroscopy to show the presence of a monodentate formate species and provide an experimental ratio for the two reaction pathways (CO_2/CO=3.9), although different from those of Inglis and Taylor.

Experimental insight into the reaction pathways is often obtained using single crystal surfaces. Toomes and King explored monolayer and multilayer potassium-promoted synthesis of surface formate and the decomposition of formic acid on Co(1010) by infrared reflective adsorption spectroscopy (IRRAS) and TPD in the temperature range of 160-640 K.[34] They found that formic acid chemisorbed onto the potassium layer forming formate and hydrogen at 160 K. The formate subsequently decomposed to CO, H_2, and atomic O above 250 K. However, surface formate could be synthesized by the reverse process, from CO, O_2, and H_2 at 300 K.

More recently, different groups provided a theoretical study of formic acid decomposition trends for several transition metal surfaces, among them Co(0001).[15,16] They focussed on the relative importance of the formate and carboxylic pathways to determine the CO_2/CO product ratio. Li *et al.* considered the reaction on Co(111) both in vacuum and with solvents[14] and then took it a step further, proposing a microkinetic analysis of the different reaction pathways on a stepped cobalt surface.[12] They found that different reaction pathways were preferred in the different cases. A more detailed discussion of the available theoretical data will be provided in comparison with our DFT calculations.

The present work provides a detailed experimental and theoretical study of the decomposition and adsorption of formic acid on Co(0001) single crystal under ultrahigh vacuum (UHV) conditions. Surface species produced during the interaction and reaction of formic acid with the surface are characterized by low energy electron diffraction (LEED), X-ray photoelectron spectroscopy (XPS) and temperature programmed desorption (TPD). Experimentally determined surface species, decomposition products and desorption energies are compared with a full density functional (DFT) calculations of energetics and transition states of the possible reaction pathways. The combination of experiment and theory is used to obtain insight on this system.

2. Experimental

Experiments were carried out in a UHV chamber with a base pressure of 3 x 10^{-10} mbar. The chamber contains an XPS, LEED, STM/AFM, mass spectrometer for TPD measurements, and has been described in detail previously.[35]

The 8 mm diameter and 0.5 mm thick cobalt single crystal sample (hcp phase) with purity of 99.999% was purchased from Princeton scientific. The (0001) crystal surface was cleaned by repetitive cycles of 10 mins of sputtering (3 keV, background pressure of 1 x 10^{-5} mbar Ar^+), followed by annealing to 600 K for 5 min. The sample was confirmed clean by LEED, shown in Figure S1 (supporting information). Temperatures above 630 K were avoided due to the Co phase transition from hexagonal closest packing (hcp) to face-centered cubic packing (fcc) at 670 K.[36,37] The sample was heated by electron bombardment and the temperature was measured by a chromel-alumel (K-type) thermocouple.

HPLC-grade formic acid (99% purity) was purchased from Sigma Aldrich. The formic acid was introduced to the UHV chamber through a leak valve that was connected to a gas manifold with a formic acid reservoir. The reservoir underwent a series of freeze-pump-thaw cycles to ensure the pressure of the gas manifold was that of the vapour pressure of formic acid. Formic acid was dosed by backfilling the chamber. The purity of the formic acid dosed was verified by a residual gas analyzer. All exposures are reported in Langmuirs (1 L = 1.0×10^{-6} torr s) without corrections for the gauge sensitivity.

2.1 XPS Measurements

XPS spectra were recorded using a standard Al Kα source (1486.7 eV) operated at 289.7 W (14.2 kV, 20.4 mA) on a Specs GmbH system (XR50 X-ray source and Phoibos 100 SCD analyzer). Selected peaks were obtained in high resolution spectra using 0.1 eV step size, 1 second dwell time, and pass energy of 20 eV. When necessary, each region was scanned 3 times to increase the signal to noise ratio. The spectra were then fit using CasaXPS analysis software using a mixed Gaussian Lorentzian function and Shirley background subtractions. Although it is tempting to consider a large number of species under each spectra, the number of curves fit was limited by the resolving peak width of the instrument (a minimum FWHM of 1.2 eV was used in all fits). The binding energy scale was calibrated using cobalt (Co 2p 3/2 = 777.8 eV).[38]

X-ray exposure was kept to the minimum required to reduce formic acid decomposition due to the X-ray beam. The clean sample was dosed with formic acid at 130 K and then heated up to the desired temperature of observation; then the spectrum was taken. Once the spectrum was finished, the sample was flashed to 630 K to clean the sample surface and verified clean by LEED. This process was repeated for each temperature of interest.

2.2 TPD Experiments

The sample surface was dosed with varying exposures of formic acid at 130 K and placed approximately 1 mm below a 1 mm diameter hole leading to a differentially pumped mass spectrometer. The temperature-controlled heating ramp was programmed in LabView and designed to provide and record a linear temperature ramp using a PID controller feedback loop. All experimental ramps started at 130 K and ended at 550 K, with a ramp rate of 4.60 ± 0.15 K/s. The sample was annealed at 630 K for 5 mins after each exposure to clean the sample. A total of 13 channels corresponding to m/z values of 46, 45, 44, 40, 32, 29, 28, 18, 17, 16, 14, 4, and 2, were monitored for the formic acid TPD experiments. These m/z values correspond to the expected species and their respective fragmentation patterns which were measured by background dosing within the instrument. All spectra were thereby correlated during analysis.

2.3 DFT Calculations

First principle calculations were performed within the framework of Density Functional Theory (DFT) using the dispersion corrected GGA functional PBE+dDsC[39–41] with the Vienna Ab

initio Simulation Package software (VASP 5.3) for electronic and geometric optimization.[42–44] The spin-polarized wave-functions were expanded on a periodic plane wave basis set with an energy cut-off of 400 eV and optimized using an energy threshold of 10^{-6} eV. The core electrons were treated using the Projection Augmented Wave (PAW) approach.[45] The electronic energy was integrated over a gamma-centered 3x3x1 Monkhorst-Pack k-point mesh.[46] For gas phase calculations, the gamma point was considered. All geometries were considered optimized when forces were less than 0.02 eV/Å.

The Co(0001) surface was modeled employing a 4 layer 3x3 periodic slab, with 5 layers void. During optimization, only the top two layers were relaxed keeping the position of the other metal atoms fixed at their bulk position. Gas phase structures were optimized in a 20x20x20 $Å^3$ simulation box.

3. Results

Experimental results will be described for adsorption of formic acid on Co(0001) using XPS, where low temperature species can be identified. Temperature programmed desorption (TPD) was used to directly observe reaction products formed both at low and high temperature. Because of the multiple regimes observed, the DFT calculation results will be presented analyzing separately the different possible reaction pathways.

3.1 X ray Photoelectron spectroscopy

Figure 1 shows the XP spectra in the carbon and oxygen regions for formic acid upon adsorption on Co(0001) at 130 K. At this temperature, the electron binding energies for the C 1s and O 1s features have been measured at 289.7 and 534.15 eV, respectively. These peak positions are characteristic of molecular formic acid on Co(0001), and are consistent with molecular adsorption at similar low temperatures on potassium-doped Co(1010)[34] and other transition metals.[11] A list of literature values for the different formic acid intermediates species is given in Table S1.

Upon heating the sample to 140 K another carbon peak evolves and the oxygen envelope becomes asymmetric. This can be attributed to the onset of formic acid undergoing decomposition and the formation of carbon monoxide. The binding energy of carbon monoxide in the carbon region is 286.2 eV,[47–49] as observed here. The oxygen peak can be partially deconvoluted taking advantage of the high binding energy component in formic acid and its oxygen stoichiometry. Thus the formic acid contribution can be isolated as shown by the two green curves in Figure 1 O1s at 140 K, with peaks at 534.15 and 533 eV. The remaining species, which include CO and other potential intermediates present, cannot be separated and are thus fitted by a single peak (blue curve in Figure 1).

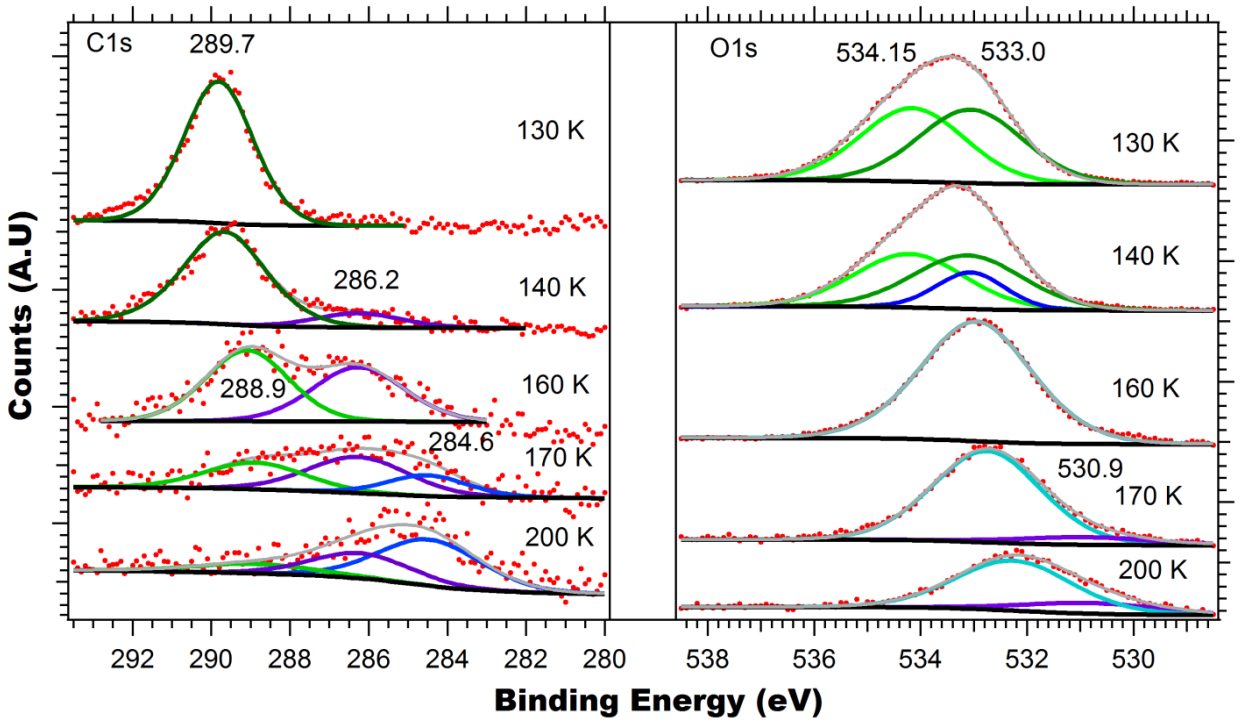

Figure 1: XPS of 1 L formic acid adsorbed at 130 K and subsequent decomposition on Co(0001). C 1s and O 1s regions shown at varying temperatures of interest. Identified peaks correspond to: i) 289.7 eV, molecular formic acid; ii) 288.9 eV, formate; iii) 286.2 eV, carbon monoxide; iv) 284.6 eV, carbon; v) 534.15 and 533 eV formic acid; vi) 530.9 eV, oxygen.

Upon heating to 160 K, there is a shift of 0.8 eV in the carbon peak, to 288.9 eV, with the corresponding disappearance of the higher energy oxygen peak, 534.15 eV, associated with formic acid. The shift in the carbon peak is in agreement with formic acid dissociation to formate and hydrogen,[50–54] and the disappearance of the higher energy oxygen peak indicates the formation of formate binding in either the bidentate or bridged orientation. Due to the disappearance of the higher energy formic acid oxygen peak, the deconvolution of the oxygen peak is no longer possible and therefore the O 1s spectrum likely corresponds to the combined signal of formate, carbon monoxide, and water species.

By 170 K, a third peak in the carbon region is observed at 284.6 eV together with a small peak in the oxygen region at 530.9 eV. At this temperature, carbon monoxide can dissociate to carbon and oxygen on Co(0001), and this process has been reported experimentally with binding energies reported at 284.3 eV and 531.0 eV,[47–49] respectively, in agreement with our observations. Note that the dissociation of CO on Co(0001) has been predicted as being extremely difficult,[55] but perhaps steps, ad-atoms, defects or a more complex mechanism is involved. Increasing the temperature up to 200 K, there is a decrease in the formate peak and a shift in the oxygen peak to 532.5 eV. The apparent shift in the oxygen peak can be explained by the fact that the adsorbed carbon monoxide to formate ratio is increasing and thus the convoluted oxygen peak is shifting

more towards the carbon monoxide binding energies. In addition, the slight decrease in the oxygen signal may be due to desorption of water in this temperature range (see TPD discussion).

Above 200 K desorption of several species becomes significant in the timeframe of XPS measurements. Thus another technique is needed to further the investigation, here temperature programmed desorption (TPD) is used.

3.2 Temperature Programmed Desorption

Temperature programed desorption spectra were obtained after deposition of formic acid on Co(0001) at 130 K. Since each molecular species produces a characteristic fragmentation pattern (multiple peaks in the mass spectrometer signal), it is possible to correct the mass spectrometer signal to correctly identify species arising from the surface as opposed to those produced by the ionization process in the mass spectrometer. As in previous work,[35,56] we have followed this procedure and all the spectra in Figure 2 have been corrected for the corresponding fragmentation patterns in the mass spectrometer and therefore reflect the actual species desorbing from the surface. The TPD spectrum of molecular formic acid, m/z 46 in Figure 2, shows negligible signal at low doses indicating the tendency of formic acid to decompose on the surface at low temperatures, as discussed above. At doses above 1 L, a very small peak around 174 K is observed, likely due to desorption of unreacted molecular formic acid. However, the main feature of the m/z 46 spectrum is a broad desorption peak with onset at 236 K. Since at this temperature all the formic acid has been decomposed (XPS result), the observation of this broad peak would indicate a second order (recombination of formate and H) desorption of the molecule.

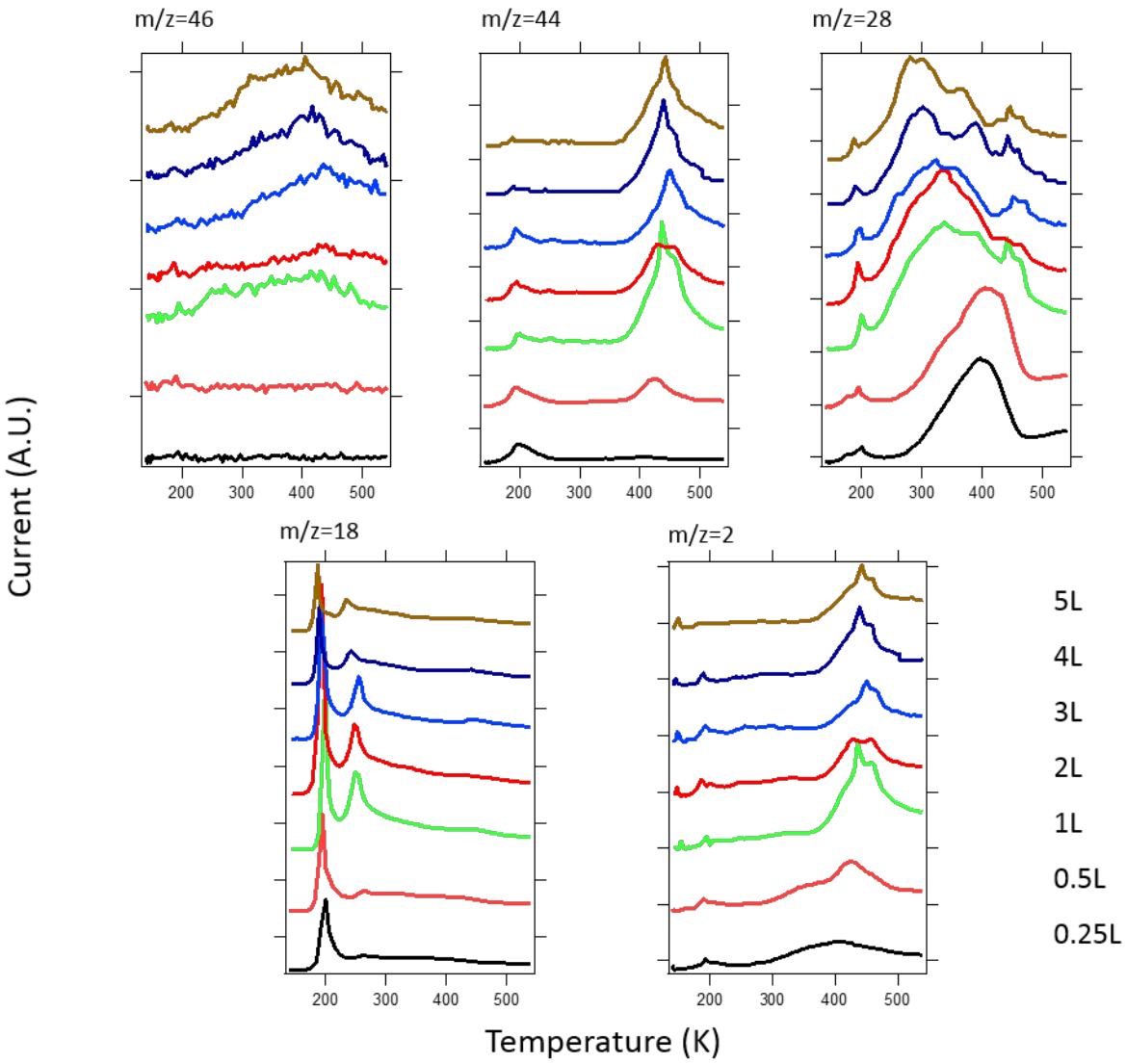

Figure 2: TPD spectra of mass/charge 46, 44, 28, 18, and 2 of increasing exposures of formic acid, dosed at 130 K, on Co(0001) under a linear temperature ramp of 4.6 K up to 550 K

The low temperature regime (below 200K), also reveals the desorption of molecular water in good agreement with the literature.[57,58] This indicates the formation of water on the surface below the peak temperature of 175 K. Additionally, upon the re-formation of formic acid on the surface at ~236 K, a second peak of water can be observed. This is obviously reaction limited (as soon as water is formed, it desorbs) giving clues for the reaction pathway of water formation (see discussion below).

Carbon monoxide can be observed to desorb in the low temperature regime. This is consistent with on-top or quasi-on-top geometries obtained at high coverages,[49,58] and in this case

caused by the constrain of other species present on the surface. However, most of the carbon monoxide, m/z 28, is observed to desorb from the surface in the range of 250 K to 400 K, in agreement with previous CO/Co(0001) studies.[47–49]

As discussed above, formate, carbon monoxide, carbon, oxygen, and water are formed and observed on the surface at low temperature and it is therefore implied that hydrogen must also be a surface species. Molecular hydrogen is expected to desorb from Co(0001) at ~370 K[59] at low coverages in a broad second order desorption peak, with the peak temperature shifting toward lower values as the coverage increases. The TPD data presented here shows a broad peak around 370 K for low coverage, however this can be attributed to ambient hydrogen deposition. No other peaks are observed below 400 K for increasing coverage suggesting that the hydrogen on the surface reacts with other species or remains on the surface below that temperature.

Analysis of all the peaks below 400 K allows for the direct determination of desorption energies at various coverages. Table 1 reports all relevant desorption energies calculated by Redhead analysis and the corrected pre-exponential factors used, calculated by the Campbell *et al.* relation.[60]

Table 1: Desorption energies of observed species, calculated by Redhead analysis.

Species	Temperature (K)	ν_{des} [a] (mbar/s)	E_{des} (kJ/mol)
Formic acid	174	1.1×10^{15}	50.2
	236[b]	1.7×10^{15}	69.5
Water	175	2.6×10^{14}	48.8
Carbon monoxide[c]	275	4.8×10^{14}	79.1
	300	5.2×10^{14}	86.7
	320	5.5×10^{14}	92.8
	380	6.5×10^{14}	111.3
	400[d]	6.9×10^{14}	117.5

[a]Pre-exponential factor derived by the method of Campbell et al.[60]

[b]Associative desorption.

[c]Molecular carbon monoxide desorption shows multiple peaks in this temperature range.[49,61]

[d]Reported associative desorption.[62,63]

At temperatures above 400 K, there appears to be a correlation in the observed signal for carbon dioxide, carbon monoxide and hydrogen. As the dose of formic acid increases from 1 to 5 L, the spectra appear to develop a triplet peak shape with main peaks at 415 K, 438 K, and 455 K. As these temperatures are above the desorption temperature of the individual molecules, these signals must be generated by a reaction taking place at that temperature (reaction limited desorption). Comparison of the yields of the three molecules was performed by not only taking into account the fragmentation patterns of all species present, but also compensating for the corresponding ionization cross sections of each species[64] in the mass spectrometer. The overall

yield of CO_2:CO:H_2 was estimated as 1:1:1 (see SI). The observation could be explained by a new reaction pathway becoming available (see discussion).

3.3 DFT Calculations

The reaction network for the decomposition of formic acid on Co(0001) has been investigated performing periodic DFT calculations on a p(3x3) slab model of the surface. Formic acid adsorbs on a top site through its carbonyl oxygen in a trans configuration in agreement with previous theoretical studies on roughened Co[12] and other metals.[16,65] The computed adsorption energy (ΔE_{ads} =-66 kJ/mol) is in reasonable agreement with the one measured by TPD (-50.2 kJ/mol, Table 1). We considered three main branches: (i) the carboxyl branch is reached through the C-H bond dissociation (ii) the formate branch through the O-H scission (iii) and the formyl branch through the C-OH bond rupture. Reaction energies and activation energies are gathered in Table 2 and shown in a complete reaction scheme in Figure S2 (supporting information). Figure 3 shows the most important reaction pathways as discussed in the text.

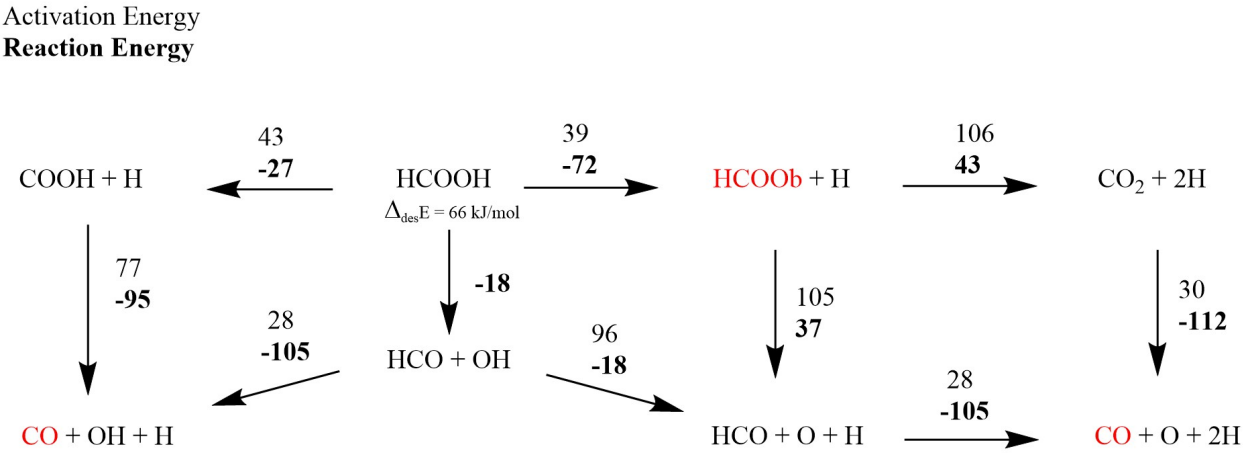

Figure 3. Schematic representation of the most relevant reaction pathways and surface species on Co(0001). Activation and reaction energies are shown. Experimentally observed species are shown in red.

Table 2. Activation and reaction energies for all processed involved in the interaction and decomposition of formic acid on Co(0001)

Label	Reaction	ΔE (kJ/mol)	ΔEa (kJ/mol)
Adsorption	HCOOH → HCOOH*	-66	n/a
	H_2 → 2 H*	-108	n/a

	H_2O → H_2O*	-44	n/a
	CO_2 → CO_2*	-3	12
	CO → CO*	-176	n/a
	O_2 → 2 O*	-495	n/a
Decomposition	HCOOH* → COOH* + H*	-27	43
	HCOOH* → $HCOO_b$* + H*	-72	39
	HCOOH* → HCO* + OH*	-18	75
	COOH* → COH* + O*	-32	89
	COOH* → CO_2* + H*	-1	97
	COOH* → CO* + OH*	-95	77
	$HCOO_b$* → $HCOO_m$*	51	52
	$HCOO_b$* → HCO + O	37	105
	$HCOO_b$* →CO_2 +H	43	106
	HCO → CO +H	-105	28
	HCO →HC + O	-65	71
	CO_2 → CO + O	-112	30
	COH → CO + H	-81	98
	COH → C + OH	10	153
	CO → C + O	73	228
	CH → C + H	32	109
Recombination	O+H → OH	18	114
	OH+H → H_2O	57	144

* indicates chemisorbed species. O2 adsorption was computed using H_2O, H_2 as a reference together with the formation energy of water (241.83 kJ/mol) to avoid using the O_2 energy, which is notoriously badly described at the GGA level.

3.3.1 Carboxyl branch

The carboxyl intermediate (COOH*) can be easily reached through the C-H bond rupture with a barrier of 43kJ/mol. The reaction is slightly exothermic (-27 kJ/mol) and co-generates a hydrogen atom adsorbed on a hollow site (H*). With its C=O bond adsorbed in a di-sigma mode, COOH* can undergo several decomposition routes. The most accessible one is the C-OH bond rupture with a barrier of 77 kJ/mol. It is strongly exothermic (-95 kJ/mol) and leaves the CO* molecule and the OH* fragment on the surface, both chemisorbed at a hollow site. CO* can hardly be dissociated into C* and O* on Co(0001) since this is a strongly endothermic and highly activated process (228 kJ/mol), in agreement with previous DFT studies.[55] The adsorption energy of CO found by DFT at this low coverage of 1/9 ML (-176 kJ/mol) is in line with previous findings but seems strongly overestimated compared with our TPD data (-117 kJ/mol at most). This discrepancy can be attributed to coverage,[6655] CO being strongly sensitive to lateral effects.[55,58] Thus, CO* does not dissociate and preferentially desorbs. The other fragment co-generated with CO* is the OH* species, which could be hydrogenated to yield water, recombining with an adsorbed hydrogen H* produced in the first step. But this reaction is endothermic (57 kJ/mol) and its high barrier (144 kJ/mol) renders this process less competitive than H_2 desorption (108 kJ/mol).

However, OH* is slightly less difficult to break than CO, with an exothermic reaction (-18 kJ/mol) that requires overcoming a barrier of 96 kJ/mol. Thus OH* tends to generate H* that desorbed as H_2 and O* that remains on the oxophilic Co(0001) surface, chemisorbed at a hollow site. The fate of the O* species is interesting to consider. Adsorbed in a hollow site, the sequential hydrogenation of O* into water is endothermic (75 kJ/mol) with high barriers (>110 kJ/mol), and therefore the process cannot compete with the H_2 desorption, which would in addition benefit from a favorable increase in temperature through a gain in entropy (ΔE_{des} = -108 kJ/mol). This is in agreement with a recent experimental study focusing on water formation on Co(0001) using surface science techniques[67] that have measured an activation energy of water formation from O* and H_2 around 129 ± 7 kJ/mol. In addition, the associative desorption of O* (yielding O_2) is strongly endothermic (495 kJ/mol), in agreement with a recent DFT study[68] on O_2 adsorption on metallic surfaces. Thus, even at a rather high temperature, O* remains on the surface while H_2 and CO desorb.

The next possible decomposition route of the carboxyl is the rupture of the C=O bond. This bond is activated by the chemisorption in a di-sigma geometry, with an elongation of 0.04 Å compared with HCOOH*. This C=O scission yields COH* and O* with a barrier of 89kJ/mol and an exothermicity of -32 kJ/mol. Then, the COH* fragment would preferentially undergo a CO-H scission, yielding CO* and H* rather than a C-OH scission according to the respective barriers of 98 kJ/mol and 153 kJ/mol. Thus, the resulting fragments are CO*, H* and O*. As already seen, CO* would rather desorb than split into C* and O*, H* will desorb as H_2 and O* will tend to stay on the Co(0001) surface.

The third possible route from COOH* is the O-H scission yielding CO_2 and H*. It is rather unlikely since it necessitates overcoming a barrier that is 20 kJ/mol higher than the C-OH bond rupture. As expected, CO_2* would easily desorb from the Co(0001) surface rather than get dissociated into CO* and O*.

3.3.2 Formate branch

Starting with the chemisorbed formic acid, the formate intermediate HCOO* can be easily reached with a barrier of 39 kJ/mol. Two main configurations of the formate can be found. In the monodentate configuration, HCOOm* is bonded through only one oxygen that bridges two surface atoms (Co-O distance of 2.03 Å). This configuration is slightly less stable that the carboxyl intermediate COOH* with an energy penalty of 21 kJ/mol. However, in its bidentate configuration, $HCOO_b$* is much more strongly stabilized by the formation of two strong Co-O bonds with a short distance of 1.99 Å. The deprotonation of formic acid HCOOH to bidentate formate is therefore particularly exothermic (-72 kJ/mol). This formate route is expected be more competitive than the carboxyl route since the OH scission barrier is slightly lower than the C-H dissociation (by 4 kJ/mol) and the obtained intermediate is much more stable (by 45 kJ/mol). Those conclusions are in line with previous DFT studies that considered the relative stability of the intermediates.[16]

HCOOb* can undergo further reaction through three different paths, however, all of them have high barriers, above 105 kJ/mol, making this intermediate a thermodynamic sink. As discussed later, these paths can only be accessed at higher temperatures. A first possibility is to re-hydrogenate the formate into formic acid with a barrier of 111 kJ/mol. Then, formic acid would easily desorb, especially at a high temperature (ΔE_{des} = 66 kJ/mol). The two others possibilities lead to the decomposition of formate into either HCO* or CO_2* with almost equal barriers (105 kJ/mol and 106 kJ/mol, respectively.). The formation of CO_2 is slightly more endothermic than the formation of HCO*. However, this step would be immediately followed by CO_2 and H_2 desorption that are both less demanding energetically than the previous rupture of the C-H bond in HCOO*. On the other hand, the generation of the formyl intermediate HCO* from $HCOO_b$* is less endothermic (37 kJ/mol) and is accompanied by the production of O* and H*. As seen previously in the carboxyl route, O* would stay on the surface while H* will desorb as H_2. HCO* would break into CO* and H* rather than CH* and O*, producing finally CO, H_2 and chemisorbed atomic oxygen O*. Indeed, the H-CO scission is easily reached with a barrier of 28 kJ/mol, the lowest of the entire network. Overall, the decomposition of the very stable formate HCOOb* produces O*, CO, H_2 and CO_2 with a limiting barrier around 105 kJ/mol.

3.3.3 Formyl branch

The chemisorbed formic acid can also undergo a C-OH dissociation yielding the formyl intermediate HCO* and OH*. This route was shown to be easily accessible on Co-stepped surface, with a barrier only slightly higher that the formate one while the last possibility, namely the C=O bond breaking was much more difficult.[12] According to our calculations, this process is more demanding on a Co(0001) surface with a barrier of 75 kJ/mol and a slight exothermicity of -18 kJ/mol. As already seen, the as-generated OH* is decomposed into O* and H* but cannot be hydrogenated into water while HCO fragments into H* and CO*. This route finally produces H_2, CO and O*. Importantly, the production of CO* requires to overcome only two low barriers (75 kJ/mol and then 28 kJ/mol).

4. Discussion

Using DFT calculations we were able to determine the energy requirements for the full reaction network on the flat Co(0001) surface. Moreover, comparison with the experimental data offers insight into the relative importance of the different pathways as conditioned by coverage or temperature. To facilitate the discussion, the results are separated into two regimes of low and high temperature (below and above 200 K) as determined by the different features of the TPD data.

4.1 Low temperature.

Formic acid was dosed on the Co(0001) surface at low temperature, and according to our XPS measurement, molecular formic acid is still the only surface species at 130 K, while chemisorbed CO* appears at a rather low temperature of 140 K and formate only forms at 160 K.

The observation of formate at this temperature is consistent with this reaction on other cobalt surfaces and other transition metals[33,69] and with the low barrier in the reaction scheme. Formation of the carboxyl species should be expected at the same time as the formate, since the two paths have similar barriers, however the carboxyl species was not observed experimentally either because its C 1s signature could not be resolved (Table S1 lists the calculated peak positions for the C 1s photoelectron for all the fragments) or because it decomposes shortly after being produced via CO formation. The disappearance of the high binding energy O 1s peak at 170 K suggests the absence of the carboxyl group. The CO formed at 140 K is seen in our TPD experiments desorbing at a temperature below 200 K. This early temperature of desorption can be related to a strong coverage effect, in this case provided by surrounding molecules and fragments. The production of CO at such low temperatures can be explained by our DFT calculations; CO can be generated together with OH* and ½ H_2 at a low temperature through either the carboxyl or the formyl path. Along the formyl path, the barriers are as low as 75 kJ/mol and the HCO* itself is not visible by XPS (within our sensitivity limits) because of its immediate decomposition to generate CO* with the lowest barrier of the whole scheme, 28 kJ/mol. Note that the HCO C1s peak would be expected at ~287.4 eV.[50,70–72] Li *et al.*[14] also note that HCO would be the preferred reaction pathway on Co(111), although in their calculations HCO was generated from HCOO* and the direct path from HCOOH was not considered. The direct path may be also facilitated by defects since the barrier is predicted to be lower on a Co-stepped surface.[12]

Our TPD experiments showed also a production of water at around 200 K. This production cannot be explained based on our DFT calculations that demonstrate that at low coverage, the formation of water from OH* and H* is very demanding energetically. This high activation energy (144 kJ/mol) might be decreased at a high coverage, however other more energetically favored processes may be at play (see section 4.3).

4.2 High temperature.

The formate species is thermodynamically favoured. That is, considering the first steps in the decomposition of HCOOH, the exothermicity ratios highly favour the HCOOb* species (HCOOb*/COOH*=2.7 and HCOOb*/HCO*=4). These ratios are consistent with previous calculations for Co(0001) (HCOOb*/COOH*=2)[16] and Co(111) (HCOOb*/COOH*=1.7).[14] Chemisorbed in a bidentate configuration, HCOOb*, it is particularly stabilized with the formation of two Co-O bonds. However, further reactions of the formate species are strongly endothermic and activated, making HCOOb* a thermodynamic sink.

The most activated process is the re-generation of formic acid that can be seen in our TPD experiments desorbing around 300-400 K. The two other routes have very close activation energies and thus yield concomitantly CO, CO_2 and H_2. This is in very good agreement with our TPD experiments that show a very similar pattern in the production of those three molecules above 400 K. As noted in the TPD section, sharp features are observed at 415, 438 and 455K for all three species suggesting that their production is simultaneous. Furthermore, the CO_2:CO ratio was

observed as roughly 1:1 for this high temperature range, consistent with the observations of Inglis and Taylor[23] above 100°C.

4.3 Water generation, a bimolecular process?

The formation of water at low temperature could not be directly explained within the reaction scheme we investigated by DFT. For that process, an alternative bimolecular reaction pathway could be the reaction of formic acid with the hydroxyl fragment OH* generated via the formyl path. This reaction would generate formate and water, an exothermic process (by 15 kJ/mol) expected to have an insignificant barrier since it involves proton transfer from a hydrogen bonded species between an acid (formic acid) and a base (adsorbed hydroxyl) The strong interaction of water and OH with formic acid and formate has previously been discussed for platinum and aluminum surfaces.[50,73–75]

An alternative is the dehydration of two formic acid molecules. This bimolecular reaction, which would generate the anhydride in gas phase, could easily produce HCOO*, HCO* and water on the Co(0001) surface (exothermic by 33 kJ/mol). The formation of a formic acid dimer or its anhydride form have been proposed and observed on other surfaces. The anhydride species, HCOOHCO, was calculated here and found to be easily dissociated with a strong exothermicity (-145kJ/mol) into HCOO* and HCO* species. Additionally, no experimental evidence of the anhydride species was observed.

5. Conclusion

This work provides mechanistic insight on the decomposition of formic acid on cobalt catalysts. Dehydration and dehydrogenation compete in the decomposition of formic acid with the ultimate formation of H_2O, CO, CO_2 and H_2. Selectivity among these products depends on the reaction mechanism and intermediates on the surface. Activation and reaction energies were calculated for the full reaction network on the Co(0001) surface, allowing the interpretation of experimental results. The adsorption and decomposition of formic acid on a Co(0001) single crystal was studied experimentally (in UHV) by XPS and TPD.

Upon adsorption of formic acid on Co(0001), three decomposition pathways have been considered, via formation of a carboxyl, a formyl or a formate species. Carbon monoxide and water are experimentally observed to be formed at low temperature. Calculations suggest that CO is formed via the formyl intermediate while water is not energetically favored on the (0001) terrace and must be produced by a bimolecular process.

The formate species is favored on the surface, being produced in a highly exothermic process and having high barriers for further decomposition. However, at high temperature, above 400 K, these decomposition paths lead to the formation of CO, CO_2 and H_2.

Acknowledgment

The authors are thankful to the LIA FunCat and the Natural Sciences and Engineering Research Council of Canada for its financial support. They also thank the Centre Blaise Pascal (CBP) and the Pôle Scientifique de Modélisation Numérique (PSMN), both at the École Normale Supérieure de Lyon, for the computational resources and technical support.

Supporting Information. LEEDs patterns for clean Co(0001), a full reaction network for the decomposition of formic acid on Co(0001), and a comparison of C1s XPS peak positions between experiment, calculations and literature is provided in the Supporting Information. XYZ positions for all the species on the surface used in the calculations provided as a separate file in SI.

References

(1) Bandara, A. Adsorption and Decomposition of Formic Acid (DCOOD) on NiO(111) and Ni(111) Surfaces Probed by SFG. *Appl. Phys. B Lasers Opt. 68* (3), 573–578.

(2) Czaun, M.; Goeppert, A.; Kothandaraman, J.; May, R. B.; Haiges, R.; Prakash, G. K. S.; Olah, G. A. Formic Acid As a Hydrogen Storage Medium: Ruthenium-Catalyzed Generation of Hydrogen from Formic Acid in Emulsions. *ACS Catal.* **2014**, *4* (1), 311–320.

(3) Bulushev, D. A. Vapour Phase Formic Acid Decomposition over PdAu/γ-Al2O3 Catalysts: Effect of Composition of Metallic Particles. *J. Catal.* **2013**, *299*, 171–180.

(4) Xu, J.; Yuan, D.; Yang, F.; Mei, D.; Zhang, Z.; Chen, Y.-X. On the Mechanism of the Direct Pathway for Formic Acid Oxidation at a Pt(111) Electrode. *Phys. Chem. Chem. Phys.* **2013**, *15* (12), 4367–4376.

(5) Angelucci, C. A.; Varela, H.; Herrero, E.; Feliu, J. M. Activation Energies of the Electrooxidation of Formic Acid on Pt(100). *J. Phys. Chem. C* **2009**, *113* (43), 18835–18841.

(6) Katano, S.; Kim, Y.; Kagata, Y.; Kawai, M. Vibration-Assisted Rotation and Deprotonation of a Single Formic Acid Molecule Adsorbed on Ni(110) Studied by Scanning Tunneling Microscopy. *J. Phys. Chem. C* **2009**, *113* (44), 19277–19280.

(7) Luo, Q.; Feng, G.; Beller, M.; Jiao, H. Formic Acid Dehydrogenation on Ni(111) and Comparison with Pd(111) and Pt(111). *J. Phys. Chem. C* **2012**, *116* (6), 4149–4156.

(8) Olson, T. S.; Pylypenko, S.; Kattel, S.; Atanassov, P.; Kiefer, B. Selectivity of Cobalt-Based Non-Platinum Oxygen Reduction Catalysts in the Presence of Methanol and Formic Acid. *J. Phys. Chem. C* **2010**, *114* (35), 15190–15195.

(9) Smith R J, B.; Loganathan, M.; Shantha, M. S. A Review of the Water Gas Shift Reaction Kinetics. *Int. J. Chem. React. Eng.* **2010**, *8* (1).

(10) Zafeiratos, S.; Dintzer, T.; Teschner, D.; Blume, R.; Hävecker, M.; Knop-Gericke, A.; Schlögl, R. Methanol Oxidation over Model Cobalt Catalysts: Influence of the Cobalt Oxidation State on the Reactivity. *J. Catal.* **2010**, *269* (2), 309–317.

(11) Columbia, M. R.; Thiel, P. A. The Interaction of Formic Acid with Transition Metal Surfaces, Studied in Ultrahigh Vacuum. *J. Electroanal. Chem.* **1994**, *369* (1–2), 1–14.

(12) Li, X.; Wang, S.; Zhu, Y.; Lv, C.; Yang, G. Density Functional Theory and Microkinetic Studies of Bio-Oil Decomposition on a Cobalt Surface: Formic Acid as a Model Compound. *Energy and Fuels* **2017**.

(13) Li, X.; Wang, S.; Zhu, Y.; Yang, G.; Zheng, P. DFT Study of Bio-Oil Decomposition Mechanism on a Co Stepped Surface: Acetic Acid as a Model Compound. *Int. J. Hydrogen Energy* **2015**, *40* (1), 330–339.

(14) Li, X.; Zhu, Y.; Chen, G.; Yang, G.; Wu, Z.; Sunden, B. Theoretical Study of Solvent Effects on the Decomposition of Formic Acid over a Co(111) Surface. *Int. J. Hydrogen Energy* **2017**.

(15) Yoo, J. S.; Abild-Pedersen, F.; Nørskov, J. K.; Studt, F. Theoretical Analysis of Transition-Metal Catalysts for Formic Acid Decomposition. *ACS Catal.* **2014**, *4* (4), 1226–1233.

(16) Herron, J. A.; Scaranto, J.; Ferrin, P.; Li, S.; Mavrikakis, M. Trends in Formic Acid Decomposition on Model Transition Metal Surfaces: A Density Functional Theory Study. *ACS Catal.* **2014**, *4* (12), 4434–4445.

(17) Columbia, M. R.; Crabtree, A. M.; Thiel, P. A. The Temperature and Coverage Dependences of Adsorbed Formic Acid and Its Conversion to Formate on Pt(111). *J. Am. Chem. Soc.* **1992**, *114* (4), 1231–1237.

(18) Columbia, M. R.; Thiel, P. A. The Reaction of Formic Acid with Clean and Water-Covered Pt(111). *Surf. Sci.* **1990**, *235* (1), 53–59.

(19) Avery, N. R. Adsorption of Formic Acid on Clean and Oxygen Covered Pt(111). *Appl. Surf. Sci.* **1982**, *11–12*, 774–783.

(20) Jeong, B.; Jeon, H.; Toyoshima, R.; Crumlin, E. J.; Kondoh, H.; Mun, B. S.; Lee, J. Dehydration Pathway for the Dissociation of Gas-Phase Formic Acid on Pt(111) Surface Observed via Ambient-Pressure XPS. *J. Phys. Chem. C* **2018**, *122* (4), 2064–2069.

(21) Kizhakevariam, N. Coadsorption of Bismuth with Electrocatalytic Molecules: A Study of Formic Acid Oxidation on Pt(100). *J. Vac. Sci. Technol. A Vacuum, Surfaces, Film.* **1990**, *8* (3), 2557.

(22) Iglesia, E.; Boudart, M. Unimolecular and Bimolecular Formic Acid Decomposition on Copper. *J. Phys. Chem.* **1986**, *90* (21), 5272–5274.

(23) Inglis, H. S.; Taylor, D. Decomposition of Formic Acid on Titanium, Vanadium, Chromium, Manganese, Iron, Cobalt, Nickel, and Copper. *J. Chem. Soc. A Inorganic, Phys. Theor.* **1969**, No. 19, 2985.

(24) Haq, S.; Love, J. G.; Sanders, H. E.; King, D. A. Adsorption and Decomposition of Formic Acid on Ni{110}. *Surf. Sci.* **1995**, *325* (3), 230–242.

(25) Mohanty, P.; Pant, K. K.; Naik, S. N.; Parikh, J.; Hornung, A.; Sahu, J. N. Synthesis of Green Fuels from Biogenic Waste through Thermochemical Route – The Role of Heterogeneous Catalyst: A Review. *Renew. Sustain. Energy Rev.* **2014**, *38*, 131–153.

(26) Hosseini, H.; Mahyari, M.; Bagheri, A.; Shaabani, A. Pd and PdCo Alloy Nanoparticles Supported on Polypropylenimine Dendrimer-Grafted Graphene: A Highly Efficient Anodic Catalyst for Direct Formic Acid Fuel Cells. *J. Power Sources* **2014**, *247*, 70–77.

(27) Yin, M.; Li, Q.; Jensen, J. O.; Huang, Y.; Cleemann, L. N.; Bjerrum, N. J.; Xing, W. Tungsten Carbide Promoted Pd and Pd–Co Electrocatalysts for Formic Acid Electrooxidation. *J. Power Sources* **2012**, *219*, 106–111.

(28) Stevanović, S.; Babić-Samardžija, K.; Sovilj, S. P.; Tripković, A.; Jovanović, V. M. Oxidation of Formic Acid on Platinum Surfaces Decorated with cobalt(III) Macrocyclic Complexes. *Russ. J. Phys. Chem. A* **2009**, *83* (9), 1442–1446.

(29) Zhang, L.; Wan, L.; Ma, Y.; Chen, Y.; Zhou, Y.; Tang, Y.; Lu, T. Crystalline Palladium–cobalt Alloy Nanoassemblies with Enhanced Activity and Stability for the Formic Acid Oxidation Reaction. *Appl. Catal. B Environ.* **2013**, *138–139*, 229–235.

(30) Stathi, P.; Deligiannakis, Y.; Louloudi, M. Co-Catalytic Enhancement of H2 Production by SiO2 Nanoparticles. *Catal. Today* **2015**, *242*, 146–152.

(31) Rice, C. Catalysts for Direct Formic Acid Fuel Cells. *J. Power Sources* **2003**, *115* (2), 229–

235.

(32) Zhou, X.; Liu, C.; Liao, J.; Lu, T.; Xing, W. Platinum-Macrocycle Co-Catalysts for Electro-Oxidation of Formic Acid. *J. Power Sources* **2008**, *179* (2), 481–488.

(33) Tang, Y.; Roberts, C. A.; Perkins, R. T.; Wachs, I. E. Revisiting Formic Acid Decomposition on Metallic Powder Catalysts: Exploding the HCOOH Decomposition Volcano Curve. *Surf. Sci.* **2016**, *650*, 103–110.

(34) Toomes, R.; King, D. Potassium-Promoted Synthesis of Surface Formate and Reactions of Formic Acid on Co {1010}. *Surf. Sci.* **1996**, No. 349, 43–64.

(35) Réocreux, R.; Ould Hamou, C. A.; Michel, C.; Giorgi, J. B.; Sautet, P. Decomposition Mechanism of Anisole on Pt(111): Combining Single-Crystal Experiments and First-Principles Calculations. *ACS Catal.* **2016**, *6* (12), 8166–8178.

(36) Lewis, W. F. Magnetic Domain Behavior during the Hcp-to-Fcc Phase Transition in Cobalt Using Lorentz Electron Microscopy. *J. Appl. Phys.* **1977**, *48* (7), 2980.

(37) Bidaux, J. E. Study of the H.c.p.-F.c.c. Phase Transition in Cobalt by Acoustic Measurements. *Acta Metall. 37* (3), 803–811.

(38) McIntyre, N. S.; Johnston, D. D.; Coatsworth, L. L.; Davidson, R. D.; Brown, J. R. X-Ray Photoelectron Spectroscopic Studies of Thin-Film Oxides of Cobalt and Molybdenum. *Surf. Interface Anal.* **1990**, *15* (4), 265–272.

(39) Perdew, J. P.; Burke, K.; Ernzerhof, M. Generalized Gradient Approximation Made Simple. *Phys. Rev. Lett.* **1996**, *77* (18), 3865–3868.

(40) Steinmann, S. N.; Corminboeuf, C. A Generalized-Gradient Approximation Exchange Hole Model for Dispersion Coefficients. *J. Chem. Phys.* **2011**, *134*, 44117.

(41) Steinmann, S. N.; Corminboeuf, C. Comprehensive Benchmarking of a Density-Dependent Dispersion Correction. *J. Chem. Theory Comput.* **2011**, *7*, 3567–3577.

(42) Kresse, G.; Hafner, J. Ab Initio Molecular Dynamics for Liquid Metals. *Phys. Rev. B* **1993**, *47*, 558–561.

(43) Kresse, G.; Furthmüller, J. Efficiency of Ab-Initio Total Energy Calculations for Metals and Semiconductors Using a Plane-Wave Basis Set. *Comput. Mater. Sci.* **1996**, *6*, 15–50.

(44) Kresse, G.; Furthmüller, J. Efficient Iterative Schemes for Ab Initio Total-Energy Calculations Using a Plane-Wave Basis Set. *Phys. Rev. B* **1996**, *54*, 11169–11186.

(45) Kresse, G.; Joubert, D. From Ultrasoft Pseudopotentials to the Projector Augmented-Wave Method. *Phys. Rev. B* **1999**, *59*, 1758–1775.

(46) Monkhorst, H. J.; Pack, J. D. Special Points for Brillouin-Zone Integrations. *Phys. Rev. B* **1976**, *13*, 5188–5192.

(47) Habermehl-Cwirzen, K.; Habermehl-Ćwirzeń, K.; Lahtinen, J. Sulfur Poisoning of the CO Adsorption on Co(0001). *Surf. Sci.* **2004**, *573* (2), 183–190.

(48) Cabeza, G. F.; Légaré, P.; Castellani, N. J. Adsorption of CO on Co (0001) and Pt – Co (0001) Surfaces : An Experimental and Theoretical Study. *Surf. Sci.* **2000**, *465* (3), 286–300.

(49) Lahtinen, J.; Vaari, J.; Kauraala, K. Adsorption and Structure Dependent Desorption of CO

on Co(0001). *Surf. Sci.* **1998**, *418* (3), 502–510.

(50) Davies, P. R.; Roberts, M. W.; Shukla, N. The Reactive Chemisorption of Formic Acid at A1(111) Surfaces and the Influence of Surface Oxidation and Coadsorption with Water: A Combined XPS and HREELS Investigation. *J. Phys. Condens. Matter* **1991**, *3* (S).

(51) Mazurkiewicz, M.; Malolepszy, A.; Mikolajczuk, A.; Stobinski, L.; Borodzinski, A.; Lesiak, B.; Zemek, J.; Jiricek, P. Pd/MWCNTs Catalytic Activity in the Formic Acid Electrooxidation Dependent on Catalyst Surface Treatment. *Phys. Status Solidi* **2011**, *248* (11), 2516–2519.

(52) Cano, E.; Torres, C.; Bastidas, J. An XPS Study of Copper Corrosion Originated by Formic Acid Vapour at 40% and 80% Relative Humidity. *Mater. Corros. UND KORROSION* **2001**, *52* (9), 667–676.

(53) Ayyoob, M.; Hegde, M. S. Electron Spectroscopic Studies of Formic Acid Adsorption and Oxidation on Cu and Ag Dosed with Barium. *J. Chem. Soc. Faraday Trans. 1 Phys. Chem. Condens. Phases* **1986**, *82* (5), 1651.

(54) Au, C. T. Adsorption and Interaction of Carbon Dioxide, Formic Acid and Hydrogen/carbon Dioxide Mixtures on (100) Zinc Oxide Surfaces Studied by Photoelectron Spectroscopy (XPS and UPS). *Surf. Sci. 199* (3), 507–517.

(55) Chen, C.; Wang, Q.; Zhang, R.; Hou, B.; Li, D.; Jia, L.; Wang, B. High Coverage CO Adsorption and Dissociation on the Co(0001) and Co(100) Surfaces from DFT and Thermodynamics. *Appl. Catal. A Gen.* **2016**, *523*, 209–220.

(56) Ould Hamou, C. A.; Réocreux, R.; Sautet, P.; Michel, C.; Giorgi, J. B. Adsorption and Decomposition of a Lignin β-O-4 Linkage Model, 2-Phenoxyethanol, on Pt(111): Combination of Experiments and First-Principles Calculations. *J. Phys. Chem. C* **2017**, *121* (18).

(57) Xu, L.; Ma, Y.; Zhang, Y.; Chen, B.; Wu, Z.; Jiang, Z.; Huang, W. Water Adsorption on a Co(0001) Surface †. *J. Phys. Chem. C* **2010**, *114* (40), 17023–17029.

(58) Jiawei, W.; Chen, J.; Guo, Q.; Su, H. Y.; Dai, D.; Yang, X. H2O and CO Coadsorption on Co (0001): The Effect of Intermolecular Hydrogen Bond. *Surf. Sci.* **2017**, *663* (April), 56–61.

(59) van Helden, P.; van den Berg, J.-A.; Weststrate, C. J. Hydrogen Adsorption on Co Surfaces: A Density Functional Theory and Temperature Programmed Desorption Study. *ACS Catal.* **2012**, *2* (6), 1097–1107.

(60) Campbell, C. T.; Árnadóttir, L.; Sellers, J. R. V. Kinetic Prefactors of Reactions on Solid Surfaces. *Zeitschrift für Phys. Chemie* **2013**, *227* (9–11), 1435–1454.

(61) Wesner, D. A.; Linden, G.; Bonzel, H. P. Alkali Promotion on Cobalt: Surface Analysis of the Effects of Potassium on Carbon Monoxide Adsorption and Fischer-Tropsch Reaction. *Appl. Surf. Sci.* **1986**, *26* (3), 335–356.

(62) Nowitzki, T.; Zielasek, V.; Baeumer, M. UHV Studies on CO and Methanol Adsorption and Decomposition on Pristine and Oxidized Alumina-Supported Co Nanoparticles. *Phys. Eng. NEW Mater. 127*, 103–112.

(63) Cabrera, A. L.; Garrido M, W. H.; Volkmann, U. G. Studies of Carbon Monoxide and

Hydrogen Adsorption on Nickel and Cobalt Foils Aimed at Gaining a Better Insight into the Mechanism of Hydrocarbon Formation. *Catal. Letters* **1994**, *25* (1–2), 115–126.

(64) Nakao, F. Determination of the Ionization Gauge Sensitivity Using the Relative Ionization Cross-Section. *Vacuum* **1975**, *25* (9–10), 431–435.

(65) Mavrikakis, M.; Dumesic, J. A.; Scaranto, J.; Singh, S.; Li, S.; Carrasquillo, R.; Roling, L.; Herron, J. A.; O'Neill, B.; Peng, G. Formic Acid Decomposition on Transition Metal Surfaces: Fundamental Mechanistic Aspects. *Abstr. Pap. Am. Chem. Soc.* **2014**, *247*.

(66) Ma, S. H.; Zu, X. T.; Jiao, Z. Y.; Zhang, X. Z. A Test of Empirical Correction to Site Preference: DFT Calculations for CO Adsorption on Co(0 0 0 1) Surface. *J. Mol. Struct. THEOCHEM* **2008**, *864* (1–3), 68–71.

(67) Kizilkaya, A. C. (Ali C.; Niemantsverdriet, J. W. (Hans); Weststrate, C. J. (Kees-J. Oxygen Adsorption and Water Formation on Co(0001). *J. Phys. Chem. C* **2016**, *120* (9), 4833–4842.

(68) Yan, M.; Huang, Z.; Zhang, Y.; Chang, C.; King, D. A.; Hu, P.; Pei, Y.; Zeng, X. C.; Flytzani-Stephanopoulos, M.; Sykes, E. C. H. Trends in Water-Promoted Oxygen Dissociation on the Transition Metal Surfaces from First Principles. *Phys. Chem. Chem. Phys.* **2017**, *19* (3), 2364–2371.

(69) Marcinkowski, M. D.; Murphy, C. J.; Liriano, M. L.; Wasio, N. A.; Lucci, F. R.; Sykes, E. C. H. Microscopic View of the Active Sites for Selective Dehydrogenation of Formic Acid on Cu(111). *ACS Catal.* **2015**, *5* (12), 7371–7378.

(70) Tanaka, K.; Matsuzaki, S.; Toyoshima, I. Photodecomposition of Adsorbed Methoxy Species by UV Light and Formaldehyde Adsorption on silicon(111) Studied by XPS and UPS. *J. Phys. Chem.* **1993**, *97* (21), 5673–5677.

(71) Bowker, M.; Madix, R. J. XPS, UPS and Thermal Desorption Studies of the Reactions of Formaldehyde and Formic Acid with the Cu(110) Surface. *Surf. Sci.* **1981**, *102* (2–3), 542–565.

(72) Frantz, P.; Kim, H. I.; Didziulis, S. V.; Li, S.; Chen, Z.; Perry, S. S. Reaction of Methyl Formate with VC(1 0 0) and TiC(1 0 0) Surfaces. *Surf. Sci.* **2005**, *596* (1–3), 144–162.

(73) Qi, Y.; Zhu, R.; Zhang, D. Adsorption Behaviors of Monomer and Dimer of Formic Acid on Pt (111) in the Absence and Presence of Water. *J. Mol. Model.* **2014**, *20* (6), 2264.

(74) Silbaugh, T. L.; Karp, E. M.; Campbell, C. T. Energetics of Formic Acid Conversion to Adsorbed Formates on Pt(111) by Transient Calorimetry. *J. Am. Chem. Soc.* **2014**, *136* (10), 3964–3971.

(75) Akiya, N.; Savage, P. E. Role of Water in Formic Acid Decomposition. *AIChE J.* **1998**, *44* (2), 405–415.

TOC Image